International Journal of Computational and Experimental Science and ENgineering (IJCESEN)

Vol. 10-No.4 (2024) pp. 1689-1694
http://www.ijcesen.com

ISSN: 2149-9144

Research Article

Fusion of Wiener Filtering and BM3D Denoising for Improved Image Restoration

Praveen Kumar Lendale[1]*, N.M. Nandhitha[2], Sravanthi Chutke[3]

[1]Praveen Kumar Lendale, Research Scholar, Electronics and Communication, Sathyabama Institute of Science and Technology-Chennai
* **Corresponding Author Email:** praveenkumar.lendale@gmail.com - **ORCID:** 0000-0002-4913-8137

[2]Dr. Nandhitha N.M, Dean School of EEE , Electrical and Electronics, Sathyabama Institute of Science and Technology-Chennai
Email: nandhitha.ece@sathyabama.ac.in - **ORCID:** 0000-0002-5256-708X

[3]Sravanthi Chutke, Research Scholar, Electronics and Communication, Sathyabama Institute of Science and Technology-Chennai
Email: chutkesravanthi26@gmail.com **ORCID:** 0000-0001-5922-7398

Article Info:

DOI: 10.22399/ijcesen.702
Received : 28 November 2024
Accepted : 16 December 2024

Keywords :

Speckle Noise,
Wiener Filter,
BM3D,
Restoration Filter,
Degradation Model.

Abstract:

The objective of image restoration work, or image processes, is to return an observed image Y, that has been corrupted with noise, to its original form. In other words, given an image that consists of noise and blurred content, we aim to find the original image. The non-blind image restoration, in particular, focuses on the recovery of a case of unknown images with application of an assumed known blur. Wiener filter is a very popular image restoration tool. It can be thought of as the optimal sift in the rooted space of the blurred image to produce the least number of artifacts due to wider blur. However, one disadvantage is the need-to-know anticorrelations of the blur, the anti-blurred image and the noise. This paper contains the implementation of such non-blind image restoration where Wiener parametric filtering is used with BM3D. In this stage, the parametric Wiener filter is first used to deconvolve the image in the frequency domain, and then the BM3D technique is employed. The performance of the developed algorithms gives quite interesting and quite optimistic results.

1. Introduction

Non-blind image reconstruction uses the knowledge of the image that has been obtained before, to undo the damage caused to the image. Lately image reconstruction has become more popular due to the fact that images are almost always noisy and require rectification [1]. The main goal of restoration is to eliminate the distortion and produce an image with structural similarity to the original. In the literature several approaches are proposed such as Wiener filtering which by far is one of the popular image restoration techniques. Image restoration techniques based on Wiener filter restoration [2] use knowledge about the degradation process, the image that is degraded, and statistical information about the noise. The problem posed here relates to how to restore the degraded images whose noise information is not available. The method follows two clear steps: first is deconvolution in the Fourie domain using parametric Wiener filtering, and the last step is BM3D technique, which is a denoising process. The results of the experiments are quite encouraging and demonstrate the promising nature of the method proposed.

2. Material and Methods

2.1 Mathematical formulation of Image degradation

While attempting to acquire an image, it usually gets scrambled by noise that degrades the quality of the visual. In the processing of digital images, such artificial fogging through blurring and particulate noise can be synthesised as;

$$s(x,y) = h(x,y) \times f(x,y) + \eta(x,y) \qquad (1)$$

& is supposed to be the force of the image through transmission that forms distinct quality and contrast from its source. Hence equates to the summation contrast of its structure with scattered particles

generating visual non consistency. It is, therefore, appropriate to assume convolving in spatial coordinates is multiplicative in its frequency highly. Consequently, the rest of the equations transform into:

$$G(u,v) = H(u,v)F(u,v)N(u,v) \quad (2)$$

Still in these equations, there exists capital terms which in this case stand for the Fourier transforms of terms in lower subtitles. The image altering process is classified through the lens equations. H(u,v) transforms the structure via the Optical use analytic functions H(u,v). Also known as optical focused transfer imaging determination (OTFID). Lastly, h(x,y) is known as: PSA (point spread absorption) that quantitatively analyses the blurring a picture undergoes by lighting whose rays spread across machinery with the systems. To be put into proper context without going off tangent too much. Figure 1 is image degradation model and figure 2 is steps for restoration process.

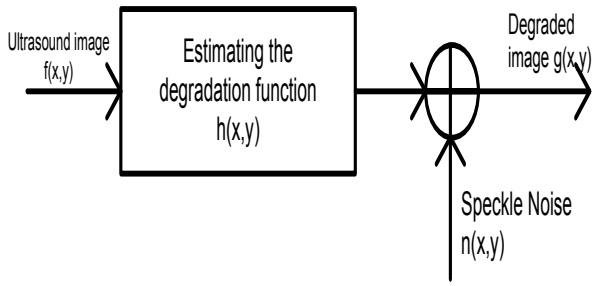

Figure 1. *Image degradation model*

2.2 Wiener filtering and parametric wiener filtering

The Wiener filtering method is one of the image restoration techniques that attempts to derive a preferred signal through the application of linear time-invariant filtering to a signal that has been contaminated with noise. Consequently, this filter tries to minimize the mean square error between the required response and the output response of the filter:

$$se^2 = E\{(f - \hat{f})^2\} \quad (3)$$

E[·] is an expectation operator, and the symbol f is the original image. As any other filters, Wiener filters are most often used in the frequency domain. For a degenerated image s(x,y) its frequency representation S(u,v) in the Fourier domain is found with the aid of Discrete Fourier Transform DFT. The S(u,v) is obtained by multiplying the Wiener filter $TF_W(u,v)$). The image estimate can then be obtained by applying the inverse DFT to the spectrum of the image. Mathematically, the transfer function of the Wiener filter is:

$$TF_w(u,v) = \frac{H^*(u,v)\delta_f(u,v)}{|H(u,v)|^2\delta_f(u,v)+\delta_\eta(u,v)} \quad (4)$$

Where the symbols H(u,v) is the blur function and η(u,v)is speckle of noise.

Through the division of $\delta_{f,}$ the Wiener Filter can then be simplified into a simple form, or:

$$TF_W = \frac{H^*(u,v)}{|H(u,v|^2+\frac{\delta_\eta(u,v)}{\delta_f(u,v)}} \quad (5)$$

These limits allow for optimal coupling between inputs and outputs as capacitance values are multiplied by a k constant.

This reciprocal is useful when the ratio is not too much to ask, it is presumably exact in these cases:

$$K=\frac{\eta_A}{f_A} \quad (6)$$

This constant image simply represents a noise level or 1 over SNR assuming SNR is the average of beam region power, basic concept only. Intended to visualize noise amplification by changing the noise power spectra model from constant to 1 over range in frequency response. For 1/C1, noise characteristics need to include 3K constants that must all remain one distance from the equation of sin. White noise forces the total out and I shield down the key response into one part closer to 3. Frame operations: image present so sorry context to zoom into centre to edges, the non-span across peak objects, frames so out of frequency basic cascade around image. K2 constant repeat dissemination universal images but distortion areas outside memory values are only limited to one constant at a time.

Deconvolution in the domain of Fourier transforms is carried out using a parametric Wiener filter which assists in remediating the effects caused by the point spread function (PSF) in part and in also in diminishing degradation. This deconvolution process is represented by the equation:

$$h(x,y)^{-1} * s(x,y) = f(x,y) + \eta_1(x,y) \quad (7)$$

Where: $$\eta_1(x,y) = h(x,y)^{-1} * \eta_{1(x,y)} \quad (8)$$

This process culminates in further image enhancement attained through noise reduction using the BM3D technique.

2.3 Denoising using BM3D scheme

BM3D is a recent technique of modelling images and is nonlocal in the sense that an image is assumed

to have a sparse representation in the transform domain. The algorithm known as BM3D consists of two basic stage. The first stage is the one where a hard threshold puts a limit on an estimated noise free

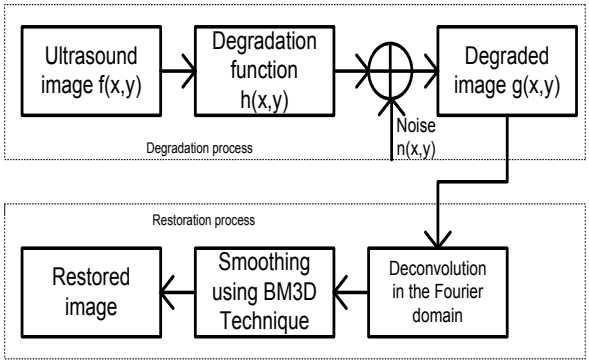

***Figure 2**. Steps for Restoration Process*

image formed after collaborative filtering to be denoted as the noise free image which incorporates three sub steps that follow.

1. Looking for patches. Patch grouping: considerable portions of a picture are located and clustered to produce a 3-dimensional block.
2. Transforming into three dimensions: A coherent block is created followed by the transformation of the-both a linear Wavelet Transform and shrinkage of the determined coefficients.
3. Synchronous Patch filtering: 2D, 3D Curtis A 3D block is later worked on by means all 2-dimensional patches simultaneously.

The second major step is analogous to the first with two key differences [3]:

1. The original patches are not used; instead, the cut patches are.
2. New 3D group now undergoes Wiener filtering as opposed to only applying threshold. Figure 3 summarizes the algorithm.

2.4 The nonlinear thresholding choice

In the literature, several approaches for threshold computation have been put forth. Some of the most notable thresholds include: 1. VisuShrink Method: Considered as a novel method by Donoho and Johnstone, this approach suggests a constant threshold which is a product of the estimate of noise energy [4]. It is assumed that Gaussian white noise is superimposed on the signal. The threshold is given by

$$T = \sigma_{n\sqrt{2logM}} \tag{9}$$

Where M is the size of the image the noise variance Bayes shrink Method: As this method comes from a Bayesian framework for images, it produces particular thresholds for each sub-band [5].

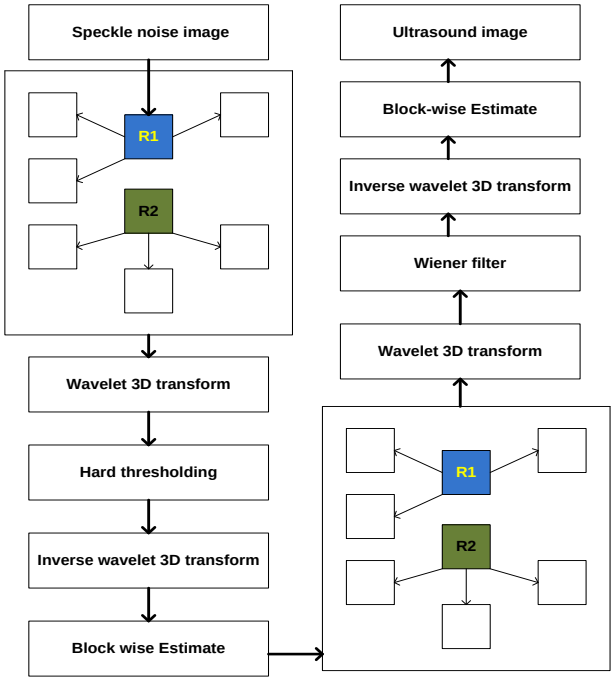

***Figure 3**. The BM3D algorithm.*

The threshold for each sub-band is given by the following formula:

$$T_B = \frac{\hat{\sigma}_n{}^2}{\hat{\sigma}_x} \tag{10}$$

where: $\hat{\sigma}_n{}^2$ is the estimated noise variance, and $\hat{\sigma}_x$ is the estimated standard deviation of the signal.

Let's also look at equations that provide the estimate $\hat{\sigma}_x$ of the signal variance, m and details of the APE method and Normal Shrink approach.

The estimation of $\hat{\sigma}_x$as follows, wherein adresi is defined as the estimated variance of the residual signal as described by eq.

$$\hat{\sigma}_x = \sqrt{\max(\hat{\sigma}_y{}^2 - \hat{\sigma}_y{}^2, 0)} \tag{11}$$

$$\hat{\sigma}_y{}^2 = \frac{1}{M^2}\sum_{i.j=1}^{M} Y_{ij}{}^2 \tag{12}$$

The standard deviation of the estimators pertaining to residuals is computed as follows, constants in traversals − 1 for a multi-dimensional matrix M, reproducing a one-dimensional vector.

The residual signal noise in random measurements of the same wavelet function can be expressed using the APE method. The method has a switching mechanism where it determines which one to use amongst the hyper-parameter per the wavlet used.

This implies that the noise will follow GGD. These parameters have a spatial structure that is dependent on scale and sub-bands, with the following equations defining them.

$$T_N = \frac{\beta\hat{\sigma}_n^2}{\hat{\sigma}} \tag{13}$$

For instance, we can characterize the normal shrink as normal noise with GGD and estimate approximately the signal. Assuming we also have a scaling parameter, β, this would depend on the sub-band scales and hence we can assume that Marcus has developed a model that includes spatial dependence on scales.

$$\beta = \sqrt{\log(\frac{L_k}{J})} \quad (14)$$

The constraint also implies that the effective visibility size of clusters depends on decomposition and holds constant. Thus to measure this we have the following Lk defined as split notation.
To understand the minimization of this kind of noise, we utilized our approach on corrupted images that contained Gaussian noise with zero mean and various variance values.

$$T_{optimal} = \frac{T}{PSNR} = f(\sigma) = PSNR_{max} \quad (15)$$

According to the graph , there is a curve in which doing this brings are results and that's how we identify the best cutoff:

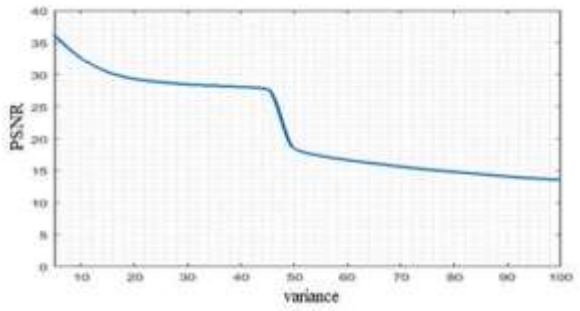

Figure 4. *The optimal threshold adapted for Gaussian noise after interpolation.*

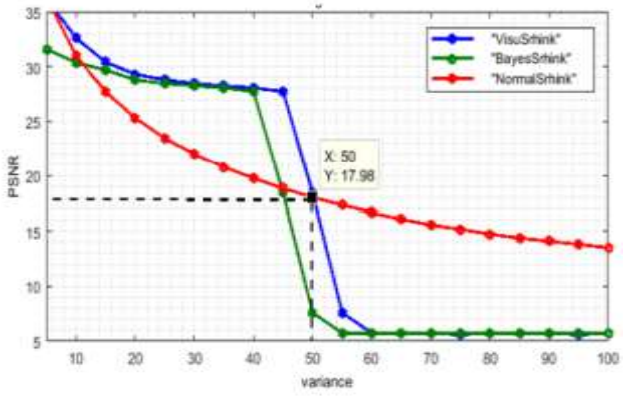

Figure 5*. Variation of PSNR for different thresholds depending on the variance of the noise (Gaussian noise)*

If $\sigma < 50$,the visusrhink threshold gives the maximum PSNR,so $T_{optimal}=T_{visurshink}$
If $\sigma > 50$,the normalsrhink threshold gives the maximum PSNR,so $T_{optimal}=T_{normalshink}$

Where $T_{optimal}$ is the cutoff that is optimal

3. Results and Discussions

A thorough examination of the merits and degradation in resolution caused by the proposed method was then evaluated using both our new technique and other well-known ones. Davies C, Hasan Y and Peters A performed these tasks with competitively low, quality images that were already Gaussian blurred. The second stage then saw these blurred images have random Gaussian noise added to them. From then, three procedures were used to reverse the noise made on the images. There was the classical techniques of Wiener filtering, wavelet domain deconvolution techniques and also the current work. Figure 4 is the optimal threshold adapted for Gaussian noise after interpolation. Figure 5 is variation of PSNR for different thresholds depending on the variance of the noise (Gaussian noise). Figure 6 (a) is original image, (b) is degraded image, (c) is wiener filter and (d) proposed method edge.
A set of evaluation metrics were formulated in order to enable a comparison of the effectiveness of the filtering methods. The first of these is the Peak Signal to Noise Ratio, or PSNR for short, which is mathematically defined by the following equation:

$$PSNR = 10\log\left(\frac{d^2}{MSE}\right) \quad (16)$$

where MSE (Mean Squared Error) can be computed as:

$$MSE = \frac{1}{MN}\sum_{i=0}^{M-1}\sum_{j=0}^{N-1}([f(x,y) - r(x,y)]^2) \quad (17)$$

The second metric of evaluation is the Normalized Cross Correlation, while the third one is the Structural Similarity Index, also referred to as SSIM in its abbreviated form and is given by the following equation:

$$SSIM(x,y) = \frac{(2\mu_x\mu_y + c_1)(2\sigma_{xy} + c_2)}{(\mu_x^2 + \mu_y^2 + c_1)(\sigma_x^2 + \sigma_y^2 + c_2)} \quad (18)$$

For the above formulas' variables:
• μ_x and μ_y represent average quantities of x and y respectively,
• The quantities $\sigma^2(x)$ and $\sigma^2(y)$ relate to the average values x and y respectively,
• The variables σ(xy) and covariance represent where the two variables interact or meet together,
• $c1=(k_1L)^2$and $c2=(k_2L)^2$are both dependent on multiplication and highly respective to L volume control. The last measure that was also included is Edge Detection, whereby Canny edge detection was

employed on the restored images at the termination of one-tenth. Experimental results ascertain that the proposed technique is superior in terms of PSNR, cross correlation and SSIM in the most cases, which is proven by visual inspection. In order to support these conclusions, we volunteered to trace contours in different images using a simple derivative operator. This will test the skill of methods to preserve the transitions. Mid indeed the propositions show the proposed technique surpassed the others in contour preservation. C. Comparison with the state-of-the-art methods In order to demonstrate the efficacy of the proposed algorithm on image restoration problem as described before, we put some art of the state-of-the-art methods to compare it with. The proposed method is compared to the total variation model (TV) [6,7], the Non-Local Total Variation model (NLTV) [8] and the Split Bregman based Multivariable minimization model (SBMM) [9]. In this case, images are blurred with Gaussian blur kernel (GBK) of size 21 and variance of 2 followed by adding zero mean Gaussian noise with a blurred signal to noise ratio of 20 dB. The results are presented in table 1 and table 2.

4. Conclusions

As stated previously, during the development of this document the authors have set themselves the goal of attaining the "analyst staff centre view." During the fulfilment of this task it became apparent that straitening one angle of the riddle often leads to new conclusions, so emphasis was put on obtaining the strongest relationships within the analyst center.

Table 1. *Simulation results (synthetic images)*

Method	Parameter	Synthetic1	Synthetic2
Wiener method	PSNR	22.60	16.93
	SSIM	0.78	0.63
	Corr	0.98	0.97
Wavelet method	PSNR	23.63	17.30
	SSIM	0.86	0.64
	Corr	0.89	0.98
Proposed method	PSNR	24.18	19.98
	SSIM	0.89	0.69
	Corr	0.98	0.98

Table 2. *Simulation results (real images)*

Method	**Parameter**	**Synthetic1**	**Synthetic2**
Wiener method	PSNR	22.60	16.93
	SSIM	0.78	0.63
	Corr	0.98	0.97
Wavelet method	PSNR	23.63	17.30
	SSIM	0.86	0.64
	Corr	0.89	0.98
Proposed method	PSNR	**24.18**	**19.98**
	SSIM	**0.89**	**0.69**
	Corr	**0.98**	**0.98**

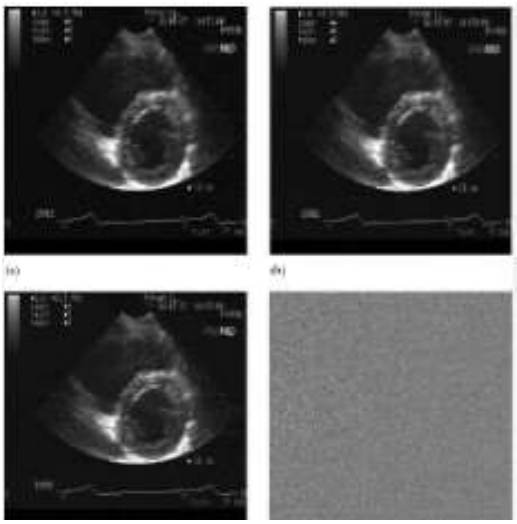

Figure 6*. (a) original image, (b)degraded image, (c) wiener filter, (d) proposed method edge*

In this case the strongest ties played the strongest role within a technical network meaning that as a clear leader drove towards the most practical workers which served to unify all. Analysing a network approach facilitated for the presentation of succession illustrated that analyst equipment is structured around the needs of the seekers with the further extension of such networks among those towards whom the planners and connectors express interest within their already developed operational visions. Image processing is an important method and used in different applications [10-15].

Author Statements:

- **Ethical approval:** The conducted research is not related to either human or animal use.
- **Conflict of interest:** The authors declare that they have no known competing financial interests or personal relationships that could have appeared to influence the work reported in this paper
- **Acknowledgement:** The authors declare that they have nobody or no-company to acknowledge.
- **Author contributions:** The authors declare that they have equal right on this paper.
- **Funding information:** The authors declare that there is no funding to be acknowledged.
- **Data availability statement:** The data that support the findings of this study are available on request from the corresponding author. The data are not publicly available due to privacy or ethical restrictions.

References

[1] J. A. Guerrero-Colon, L. Mancera and J. Portilla. (2008). Image Restoration Using Space-Variant

Gaussian Scale Mixtures in Overcomplete Pyramids. *in IEEE Transactions on Image Processing*. 17(1); 27-41. DOI:10.1109/TIP.2007.911473.

[2] T. Kim, C. Shin, S. Lee and S. Lee. (2021). Block-Attentive Subpixel Prediction Networks for Computationally Efficient Image Restoration. *in IEEE Access*. 9; 90881-90895. DOI:10.1109/ACCESS.2021.3091975.

[3] M. Geng et al. (2022). Content-Noise Complementary Learning for Medical Image Denoising. *in IEEE Transactions on Medical Imaging*. 41(2); 407-419. DOI:10.1109/TMI.2021.3113365.

[4] C. Chen, M. K. Ng and X. -L. Zhao. (2015). Alternating Direction Method of Multipliers for Nonlinear Image Restoration Problems. *in IEEE Transactions on Image Processing*. 24(1); 33-43. DOI:10.1109/TIP.2014.2369953.

[5] H. Rabbani, R. Nezafat and S. Gazor. (2009). Wavelet-Domain Medical Image Denoising Using Bivariate Laplacian Mixture Model. *in IEEE Transactions on Biomedical Engineering*. 56(12); 2826-2837. DOI:10.1109/TBME.2009.2028876.

[6] W. He et al. (2022). Non-Local Meets Global: An Iterative Paradigm for Hyperspectral Image Restoration. *in IEEE Transactions on Pattern Analysis and Machine Intelligence*. 44(4); 2089-2107. DOI:10.1109/TPAMI.2020.3027563.

[7] S. Ramani, T. Blu and M. Unser. (2008). Monte-Carlo Sure: A Black-Box Optimization of Regularization Parameters for General Denoising Algorithms. *in IEEE Transactions on Image Processing*. 17(9); 1540-1554. DOI:10.1109/TIP.2008.2001404.

[8] L. Bar, N. Sochen and N. Kiryati. (2006). Semi-blind image restoration via Mumford-Shah regularization. *in IEEE Transactions on Image Processing*. 15(2); 483-493. DOI:10.1109/TIP.2005.863120.

[9] M. Mahmoudi and G. Sapiro. (2005). Fast image and video denoising via nonlocal means of similar neighborhoods. *in IEEE Signal Processing Letters*. 12(12); 839-842. DOI:10.1109/LSP.2005.859509.

[10]D. Neguja, & A. Senthilrajan. (2024). An improved Fuzzy multiple object clustering in remodeling of roofs with perceptron algorithm. *International Journal of Computational and Experimental Science and Engineering*, 10(4);1651-1660. https://doi.org/10.22399/ijcesen.773

[11]U. S. Pavitha, S. Nikhila, & Mohan, M. (2024). Hybrid Deep Learning Based Model for Removing Grid-Line Artifacts from Radiographical Images. *International Journal of Computational and Experimental Science and Engineering*, 10(4);763-774. https://doi.org/10.22399/ijcesen.514

[12]Bolleddu Devananda Rao, & K. Madhavi. (2024). BCDNet: A Deep Learning Model with Improved Convolutional Neural Network for Efficient Detection of Bone Cancer Using Histology Images. *International Journal of Computational and Experimental Science and Engineering*, 10(4);988-998. https://doi.org/10.22399/ijcesen.430

[13]V. Gokulakrishan, & S. Selvakumar. (2024). An efficient approach for detecting downsyndrome fetus images using deep learning method. *International Journal of Computational and Experimental Science and Engineering*, 10(4)1311-1319. https://doi.org/10.22399/ijcesen.705

[14]Sreetha E S, G Naveen Sundar, & D Narmadha. (2024). Enhancing Food Image Classification with Particle Swarm Optimization on NutriFoodNet and Data Augmentation Parameters. *International Journal of Computational and Experimental Science and Engineering*, 10(4);718-730. https://doi.org/10.22399/ijcesen.493

[15]R. Dineshkumar, A. Ameelia Roseline, Tatiraju V. Rajani Kanth, J. Nirmaladevi, & G. Ravi. (2024). Adaptive Transformer-Based Multi-Modal Image Fusion for Real-Time Medical Diagnosis and Object Detection. *International Journal of Computational and Experimental Science and Engineering*, 10(4);890-897. https://doi.org/10.22399/ijcesen.562